CONTRACT TECHNICAL REPORT
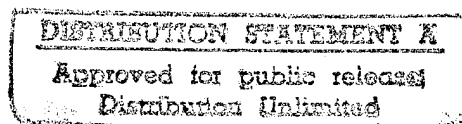
"The Immersed Fatigue Response of Polymer Composites"

By

L. V. Smith and Y. J. Weitsman

19960201 040

DTIC QUALITY INSPECTED 8

**Mechanical and Aerospace Engineering
    and Engineering Science**
THE UNIVERSITY OF TENNESSEE
Knoxville, TN   37996-2030

UT

REPORT DOCUMENTATION PAGE

1a. REPORT SECURITY CLASSIFICATION		1b. RESTRICTIVE MARKINGS			
Unclassified					

2a. SECURITY CLASSIFICATION AUTHORITY	3. DISTRIBUTION/AVAILABILITY OF REPORT
	Unlimited DISTRIBUTION STATEMENT A
2b. DECLASSIFICATION/DOWNGRADING SCHEDULE	Approved for public release; Distribution Unlimited

4. PERFORMING ORGANIZATION REPORT NUMBER(S)	5. MONITORING ORGANIZATION REPORT NUMBER(S)

6a. NAME OF PERFORMING ORGANIZATION	6b. OFFICE SYMBOL (If applicable)	7a. NAME OF MONITORING ORGANIZATION
Mechanical & Aerospace Eng. & Eng. Sci. University of Tennessee		Office of Naval Research

6c. ADDRESS (City, State and ZIP Code)	7b. ADDRESS (City, State and ZIP Code)
307 Perkins Hall Knoxville, TN 37996-2030	Office of Naval Research, Code 432 800 N. Quincy Ave., BCT #1, Room 528 Arlington, VA 22217

8a. NAME OF FUNDING/SPONSORING ORGANIZATION	8b. OFFICE SYMBOL (If applicable)	9. PROCUREMENT INSTRUMENT IDENTIFICATION NUMBER
Office of Naval Research		N00014-90-J-1556 (ONR Contract #)

8c. ADDRESS (City, State and ZIP Code)	10. SOURCE OF FUNDING NOS.			
	PROGRAM ELEMENT NO.	PROJECT NO.	TASK NO.	WORK UNIT NO.
Arlington, VA 22217				

11. TITLE (Include Security Classification) The Immersed Fatigue Response of Polymer Composites

12. PERSONAL AUTHOR(S)
L. V. Smith and Y. J. Weitsman

13a. TYPE OF REPORT	13b. TIME COVERED	14. DATE OF REPORT (Yr., Mo., Day)	15. PAGE COUNT
Technical	FROM 10/1/92 TO 2/1/96	96-01-02	26

16. SUPPLEMENTARY NOTATION

17.	COSATI CODES		18. SUBJECT TERMS (Continue on reverse if necessary and identify by block number)
FIELD	GROUP	SUB. GR.	

19. ABSTRACT (Continue on reverse if necessary and identify by block number)

The effect of sea water on carbon/epoxy cross ply specimens is studied by consideration of fatigue data and failure modes. Tests were conducted using dry and saturated coupons fatigued in air, as well as pre-saturated coupons fatigued while immersed in sea water. The saturated coupons fatigued in air had the longest fatigue life, which was attributed to stress relief from sorption induced swelling. Saturated coupons fatigued in an immersed environment exhibited the shortest fatigue life, and also experienced significant delaminations prior to failure. Water trapped inside the transverse cracks during the load cycle provides a physical mechanism explaining this behavior. An analytical and numerical analyses are presented which show how moisture inside the transverse cracks can alter the coupon stress state and enhance delamination.

20. DISTRIBUTION/AVAILABILITY OF ABSTRACT	21. ABSTRACT SECURITY CLASSIFICATION	
UNCLASSIFIED/UNLIMITED ☐ SAME AS RPT. ☐ DTIC USERS ☐	Unclassified	
22a. NAME OF RESPONSIBLE INDIVIDUAL	22b. TELEPHONE NUMBER (Include Area Code)	22c. OFFICE SYMBOL
Dr. Yapa Rajapakse	(703) 696-4405	

DD FORM 1473, 83 APR   EDITION OF 1 JAN 73 IS OBSOLETE.

THE IMMERSED FATIGUE RESPONSE OF POLYMER COMPOSITES

L. V. Smith

Y. J. Weitsman

University of Tennessee

Knoxville, Tennessee

ABSTRACT

The effect of sea water on carbon/epoxy cross ply specimens is studied by consideration of fatigue data and failure modes. Tests were conducted using dry and saturated coupons fatigued in air, as well as pre-saturated coupons fatigued while immersed in sea water. The saturated coupons fatigued in air had the longest fatigue life, which was attributed to stress relief from sorption induced swelling. Saturated coupons fatigued in an immersed environment exhibited the shortest fatigue life, and also experienced significant delaminations prior to failure. Water trapped inside the transverse cracks during the load cycle provides a physical mechanism explaining this behavior. An analytical and numerical analyses are presented which show how moisture inside the transverse cracks can alter the coupon stress state and enhance delamination.

1. INTRODUCTION

Effects of fluids in polymers and their composites have been studied extensively over the past several decades. A recent review of the literature illustrates this point (Weitsman, 1995). In general, absorbed fluids are known to degrade the strength, stiffness, and durability of polymeric materials, and accelerate the time-dependent processes. These degradations were observed to increase in the presence of synergistic mechanisms.

While the fatigue behavior of polymeric composites has been studied extensively in the literature, the topic of wet fatigue has received comparatively little attention. Furthermore, investigations that concerned fatigue considered

1

saturated coupons fatigued in air (Dewimille et al. 1980, Friedrich and Karger-Kocsis 1990, Phillips et al. 1987, Sandifier 1982, Sumsion 1976, Yang et al. 1992). The current study presents fatigue data for dry and saturated coupons tested in air and while immersed in sea water. It is shown that capillary effects associated with immersed fatigue play a significant role in the failure process. Results from analytical and numerical models are presented that compare the stress fields and delamination fracture energy for dry and saturated coupons fatigued in air and sea water and explain the observed fatigue life and failure mode.

2. EXPERIMENTAL

The experiments subjected standard tensile coupons 25 mm wide and 200 mm long to tension-tension fatigue. Specimens were fabricated from AS4/3501-6 prepreg in a $[0/90_3]_s$ eight ply lay-up. Coupons were saturated by immersion in a 30°C sea water bath for a minimum of four months, after which the incremental weight gain became negligible. The bath was heated to expedite the saturation process.

Tensile testing of both dry and saturated coupons reveal that transverse cracks form in the 90° plies at relatively low loads. This provides a mechanism for capillary action in the transverse cracks during immersed fatigue, which is shown schematically in
Fig. 1. Capillary climb was measured using an x-ray penetrant and a slightly acidic water solution. Transverse cracks were formed in coupons by cycling them twice to loads ranging from 74 to 90% of their ultimate tensile strength. In the x-ray experiments coupons were placed in a shallow bath of x-ray penetrant, with the cracks oriented vertically, as represented in Fig. 2. X-ray images of these coupons were then taken at 1 minute intervals, from which the rate of capillary climb was continuously measured. A similar technique was undertaken using an acidic solution. In the latter case litmus paper, which was placed over the top edge of the coupon, changed color in the cracked areas. In both tests, and for all stress levels, the rate of capillary climb was approximately 0.7 cm/min.

Fatigue testing was carried out at 5 Hz with $R = \overline{\sigma_x}^{min} / \overline{\sigma_x}^{max} = 0.1$. Coupons were tension-tension fatigued at 74, 79, 84 and 89% of their ultimate tensile strength

(σ_u=540 MPa) in three conditions: (a) dry coupons tested in air; (b) saturated coupons tested in air; (c) saturated coupons tested while immersed in sea water. S-N data (Kosuri and Weitsman, 1995) are presented in Fig. 3 where saturated coupons fatigued in air are observed to have a consistently longer fatigue life than the other two test conditions. This is likely due to sorption induced swelling, which counters the shrinkage generated during the post-processing cool-down. Immersed fatigue of saturated coupons appears to shorten the fatigue life significantly, reducing it to levels that lie below those that correspond to saturated and dry coupons fatigued in air.

Photographs of representative failed specimens are presented in Fig. 4. As shown in the figure, saturated coupons were observed to have significantly fewer transverse cracks than the dry case, which may be attributed to stress relief from sorption induced swelling. On the other hand, coupons tested while immersed exhibited more extensive delaminations than the dry fatigue coupons. It is believed that the delamination and reduced fatigue life of saturated coupons exposed to immersed fatigue is caused by a synergistic effect between water drawn by capillary action and cyclic mechanical loading.

3. ANALYSIS

The experimental observations presented above have prompted an investigation of the combined effects of load and moisture on composite laminates with transverse cracks. The intent of this study is to explain how moisture and load act synergistically to reduce the fatigue life and increase delamination.

In order to examine the combined effects of sorption, immersion and load, their independent effects must be separated. This may be done by considering the relative time scale on which each is occurring. For the coupons considered in this study, sorption processes require about $t_s = 15\times10^4$ minutes to reach steady state, capillary action through the width of the coupon is complete in approximately $t_c = 5$ minutes, while at a fatigue rate of 5 Hz, the load cycle requires just $t_l = 3\times10^{-3}$ minutes.

In the analysis presented below, inertia effects related to dynamic loading are neglected and quasi-static loading is considered. It is assumed that water is drawn by capillary action into the cracks through a random walk process. The mass of water inside the crack is determined from the crack opening displacement at $\overline{\sigma}_x^{max}$. In view of the vast disparity between the time-scales for capillary motion and load cycling ($t_1/t_c \sim 6\times10^{-4}$) it is assumed that the foregoing mass of water is preserved during the loading cycle. Compressibility of water inside the crack is taken into account, as are non-mechanical strains due to post-processing thermal shrinkage and sorption swelling.

3.1 SHEAR LAG ANALYSIS

A comparative study of the stress fields which correspond to the three foregoing fatigue conditions was conducted using a shear lag analysis. The model employed here is taken from Nuismer and Tan (1988), with the geometry as shown in Fig. 5. Stresses are averaged through the thickness and examined as a function of position, x. Additionally, it is assumed that $\sigma_z = 0$ (plane stress), τ_{zx} and τ_{zy} are linear in z, and $\partial w/\partial x = 0$ (no bending). In the sequel let an "over-bar" denote an average quantity, namely $\overline{f}^{(k)}(x) = \int_0^h f^{(k)}(z,x)dz$. Symmetry at x = 0 produces the displacement boundary conditions: $\overline{u}^{(90)}(0) = \overline{u}^{(0)}(0) = 0$. For the case of immersed fatigue, the boundary condition at x = L differs from that used by Nuismer and Tan, since they considered traction free crack surfaces. Accounting for a pressure p at the transverse crack surface we have: $\overline{\sigma}^{(90)}(L) = -p$, $\overline{\sigma}^{(0)}(L) = \dfrac{\overline{\sigma}_x h + p h_{90}}{h_0}$, where $\overline{\sigma}_x$ is the average value of the applied stress. Since the methodology of shear lag analysis is well documented the details will be omitted here. Substitution of the above boundary conditions and solving for the stress fields produces the following expressions for the 0° and 90° ply groups:

$$\overline{\sigma}_x^{(90)}(x) = \frac{\tau^{*}(L)}{h_{90}\alpha_1^2}\left[1 - \frac{\cosh(\alpha_1 x)}{\cosh(\alpha_1 L)}\right] - p \tag{1}$$

4

$$\bar{\sigma}_x^{(0)}(x) = \frac{1}{h_0}\left[\bar{\sigma}_x h - \bar{\sigma}_x^{(90)} h_{90}\right] \tag{2}$$

where

$$\tau^*(L) = \frac{A_{55}}{h}\left\{\frac{1}{Q_{11}^{(0)}}\left[\frac{(\bar{\sigma}_x h + p h_{90})}{h_0} + \sigma_{xN}^{(0)} - Q_{12}^{(0)}\bar{\varepsilon}_y\right] - \frac{1}{Q_{11}^{(90)}}\left[\sigma_{xN}^{(90)} + Q_{12}^{(90)}\bar{\varepsilon}_y - p\right]\right\} \tag{3}$$

with

$$A_{55} = \frac{3h G_{TT} G_{LT}}{h_{90} G_{LT} + h_0 G_{TT}} \tag{4}$$

and

$$\alpha_1^2 = \frac{A_{55}}{Q_{11}^{(90)} Q_{11}^{(0)} h}\left[\frac{Q_{11}^{(90)}}{h_0} + \frac{Q_{11}^{(0)}}{h_{90}}\right]. \tag{5}$$

G_{LT} and G_{TT} are the shear moduli, Q is the two dimensional stiffness matrix, and σ_{xN} denotes the non-mechanical stress within the 0° or 90° ply group as indicated by the superscript. The only remaining unknown at this stage is the transverse strain, $\bar{\varepsilon}_y$. As a first order approximation it can be neglected. However, in the absence of transverse forces, $\bar{\varepsilon}_y$ can be found from:

$$N_y = \int_0^L \left[h_{90}\bar{\sigma}^{(90)} + h_0\bar{\sigma}^{(0)}\right]dx = 0 \tag{6}$$

Evaluation of (6) results in a simple, but lengthy expression for $\bar{\varepsilon}_y$, which is typically solved through iteration.

All coupons were given a thermal shrinkage strain associated with a post-processing temperature drop of 125°C. Saturated coupons were given a swelling strain which corresponds to a 1.7% weight gain. In the analysis the following material properties were used: $E_1 = 139$ GPa, $E_2 = E_3 = 11$ GPa, $v_{12} = v_{13} = 0.27$, $v_{23} = 0.34$, $G_{LT} = 4.8$ GPa, $G_{TT} = E_3/2(1+v_{23})$, $\alpha_1^T = -0.9\mu\varepsilon/°C$, $\alpha_2^T = 31\mu\varepsilon/°C$, $\beta_1 = 100\mu\varepsilon/\%\Delta w$, $\beta_2 = 3200\mu\varepsilon/\%\Delta w$. A lamina thickness of 0.125 mm and crack spacing of L = 1 mm were also used. Applied stresses ranged from $\bar{\sigma}_x^{min} = 45$ MPa to $\bar{\sigma}_x^{max} = 450$ MPa.

Results were obtained for the three conditions, namely: dry coupons tested in air, saturated coupons tested in air, and saturated coupons tested immersed. For coupons tested in air the transverse crack pressure was set to zero. A value for $\bar{\varepsilon}_y$

5

was assumed, and the stress field was found from (1) and (2). A new value for $\bar{\varepsilon}_y$ was found from the solution of (6) which value was then used in (3) and subsequently (1) and (2). This procedure was repeated until $\bar{\varepsilon}_y$ converged.

For coupons tested immersed, the volume of water in the crack was found from the crack opening at the maximum applied load, as given by

$$\bar{u}_{\max} = \bar{u}^{(0)}\left(L, \bar{\sigma}_x^{\max}\right) - \bar{u}^{(90)}\left(L, \bar{\sigma}_x^{\max}\right), \tag{7}$$

with $p = 0$. For brevity the expressions for $\bar{u}^{(k)}$, which are contained in the shear lag solution, are not presented here. At some intermediate stress level $\left(\bar{\sigma}_x < \bar{\sigma}_x^{\max}\right)$ a pressure p was guessed from which a crack opening would be found according to

$$\bar{u} = \bar{u}^{(0)}\left(L, \bar{\sigma}_x\right) - \bar{u}^{(90)}\left(L, \bar{\sigma}_x\right). \tag{8}$$

Assuming water to be linearly compressible (7) and (8) can be related to p by:

$$p = \frac{\bar{u}_{\max} - \bar{u}}{\bar{u}_{\max}} k \tag{9}$$

where a bulk modulus of water, $k = 2.5$ GPa, was used. This new value of p would then be used to find a new $\bar{u}$, until p converged.

The stress fields in the 0° ply group for the three conditions at $\bar{\sigma}_x^{\max}$ are presented in Fig. 6. The stress fields for the two saturated cases coincide since there is no pressure inside the crack at $\bar{\sigma}_x^{\max}$. The effect of the water-induced residual stress is observed in the figure, where it lowers the load transfer from the 0° ply group to the 90° ply group. Fig. 7 presents the stress fields for the 0° ply group at $\bar{\sigma}_x^{\min}$. For the circumstance of saturated coupons fatigued in air, the crack at x = L happens to close, producing uniform stress. As indicated by (1), pressure applied to the surface of the transverse crack vertically shifts the stress field by p.

Stresses in the 90° ply group at $\bar{\sigma}_x^{\max}$ and $\bar{\sigma}_x^{\min}$ are presented in Fig. 8 and Fig. 9 respectively. Perhaps unexpectedly, Fig. 9 indicates that for the immersed case the 90° ply group is completely in compression. Immersed tension-tension fatigue of coupons with transverse cracks, therefore, has the potential of producing tension-compression cyclic stresses within portions of the coupon.

6

3.2 FINITE ELEMENT ANALYSIS

A comparative study of the delamination fracture behavior was conducted using finite elements. The modified crack closure integral approach used here is as described by Rybicki and Kanninen (1977). The geometry of a delaminated transverse crack is presented in Fig. 10. Taking advantage of symmetry it suffices to consider a quarter of the region shown in Fig. 10. Subsequently, the geometry was meshed in Abaqus using four noded quadrilateral elements. Strain energy release rates were found by consideration of nodal forces, displacements, and spatial coordinates adjacent to the crack root according to:

$$G_I = \lim_{\Delta c \to 0} \frac{F \Delta v}{2 \Delta c} \tag{10}$$

$$G_{II} = \lim_{\Delta c \to 0} \frac{T \Delta u}{2 \Delta c} \tag{11}$$

Where G_I, G_{II} denote levels of available mode I and mode II fracture energies, F and T are normal and tangential forces at the crack root required to hold the crack closed, and Δu and Δv are relative displacements of the crack surfaces a distance Δc from the crack root. In the analysis plane strain assumptions were invoked, and non-mechanical strains were input via equivalent thermal expansion by lumping moisture and thermally induced swelling effects.

Strain energy release rates were obtained directly from this model for the two cases of dry and saturated coupons fatigued in air. An iterative procedure was implemented to determine the magnitude of the uniform pressure acting along the face of the transverse crack for the case of immersed fatigue. A maximum crack opening area, A_{max}, was found at $\overline{\sigma_x}^{max}$ with $p = 0$. At an intermediate stress level, a pressure p was guessed from which a crack opening area, A, was found. Pressure was then related to the change in area by:

$$p = \frac{A_{max} - A}{A_{max}} k \tag{12}$$

7

where, as before, $k = 2.5$ GPa is the bulk modulus of water. This new value of p was then used in the next iteration to find a new A until p converged. Convergence to within 1% was typically achieved after three iterations.

Fig. 11 presents the total strain energy release rate, G_{tot}, as a function of applied stress for a delamination length of a = 0.125 mm, and a crack spacing of L = 5 mm. For the two cases of fatigue in air G_{tot} is observed to increase with applied stress, while for the case of immersed fatigue, G_{tot} decreased with $\bar{\sigma}_x$ (it increased with pressure). While it is expected that G_{tot}^{max} is lowest for the case of saturated coupons fatigued in air, it may be noted that G_{tot}^{max} of the remaining two conditions is similar in magnitude.

Fig. 12 presents the mode I strain energy release rate, G_I, as a function of applied stress, which should provide a better criterion for delamination. It is apparent that delaminations of saturated coupons fatigued while immersed occur primarily in mode I ($G_{tot} \approx G_I$), the other two cases are subjected to mode II fracture. Since $G_{IIc} > 2G_{Ic}$ for most carbon-epoxy composites (Whitney, 1990) increased delamination is expected for the saturated coupons fatigued while immersed.

G_{tot}^{max} has been plotted as a function of delamination length, a, in Fig. 13. For the two cases of fatigue in air, G_{tot}^{max} occurs at $\bar{\sigma}_x^{max}$, while for immersed fatigue, G_{tot}^{max} occurs at $\bar{\sigma}_x^{min}$, or equivalently, at $p = p_{max}$. However, a much better insight may be gained by observing the maximum mode I strain energy release rate as plotted versus delamination length in Fig. 14. This figure provides a clear indicator that under immersed conditions the energy available for delamination growth increases with delamination length. This synergistic mechanism explains the extensive delaminations shown in the top of Fig. 4 for the immersed fatigue case.

4. SUMMARY

A series of fatigue tests in air and while immersed have been conducted on dry and saturated coupons. It was noted that saturated coupons fatigued in air exhibited the longest fatigue life and saturated coupons fatigued while immersed in sea water failed after the shortest number of load cycles. Further, reduced transverse

cracking and increased delamination were observed in the case of saturated coupons fatigued while immersed.

Comparative stress fields for the three foregoing test conditions were evaluated using a shear lag analysis. Water trapped inside transverse cracks during immersed fatigue was included in the analysis. Sorption and immersed fatigue were observed to affect the coupon stress state, where the latter gave rise to cyclic tension-compression internal stresses in spite of the external tension-tension fatigue loading. Delamination fracture energy was compared for the three test conditions using finite elements. The total fracture energy was lowest for saturated coupons fatigued in air for all ranges of applied stress and delamination considered. While the maximum total fracture energies of dry coupons fatigued in air and saturated coupons fatigued immersed were comparable, the latter was nearly entirely of mode I, while the former was mostly of mode II. Given the lower critical strain energy release rate in mode I, these results explain the observed extensive delaminations and shorter fatigue life associated with immersed fatigue.

5. ACKNOWLEDGMENT

REFERENCES

Dewimille, B.; Thoris, J.; Mailfert, R.; Bunsell, A. R. 1980. "Hydrothermal aging of an unidirectional glass-fibre epoxy composite during water immersion." A. R. Bunsell, C. Bathias, A. Martrenchar, D. Menkes and G. Verchery (eds.) Proceedings of the Third International Conference on Composite Materials:597-612.

Friedrich, K. and Karger-Kocsis, J. 1990. "Fracture and fatigue of unfilled and reinforced polyamides and polyesters." J. M. Schults and S. Fakirov (eds.) Solid Sate Behavior of Linear Polyesters and Polyamides: 249-322. Prentice-Hall.

Nuismer, R. J. and Tan, S., C. 1988. "Constitutive relations of a cracked composite lamina." Journal of Composite Materials. 22:306-321.

Phillips, D. C.; Scott, J. M.; Buckley, N. 1987. "The effects of moisture on the shear fatigue of fibre composites." B. Noton, R. Signorelli, K. Street and L. Phillips (eds.), ICCM/2 Proceedings of the 1978 International Conference on Composite Materials: 1544-1559.

Sandifier, J. P. 1982. "Effects of corrosive environments on graphite/epoxy composites." T. Hayashi, K. Kawata and S. Umekawa (eds.), Proceedings of the Fourth International Conference on Composite Materials:979-986.

Sumsion, H. T. 1976. "Environmental effects on graphite-epoxy fatigue properties. Journal of Spacecrafts and Rockets, 13:150-155.

Kosuri, R. and Weitsman, Y. 1995. "Sorption processes and immersed fatigue response of gr/ep composites in sea water." Proceedings of the ICCM-10, Whistler, British Columbia, Canada. 4:177-184

Rybicki, E. F. and Kanninen, M. F. 1977. "A finite element calculation of stress intensity factors by a modified crack closure integral." Engineering Fracture Mechanics. 9:931-938.

Weitsman, Y. 1995. "Effects of fluids on polymeric composites-a review." Report No. MAES 95-1.0 CM, Department of Aerospace and Mechanical Engineering and Engineering Science, University of Tennessee, Knoxville, TN.

Whitney, J. M. 1990. "Interlaminar Fracture." International Encyclopedia of Composites, S. M. Lee (ed.), VCH Publishers, 2:289-306.

Yang, B.-X.; Kasamori, M.; and Yamamto, T. 1992. "The effect of water on the interlaminar delamination growth of composite laminates." C. T. Sun and T. T. Loo (eds.), Proceedings of the Second International Symposium on Composite Materials and Structures: 334-339.

LIST OF FIGURES

fatigued while immersed in sea water. (For a crack spacing of 10 mm and delamination of 0.125 mm.)

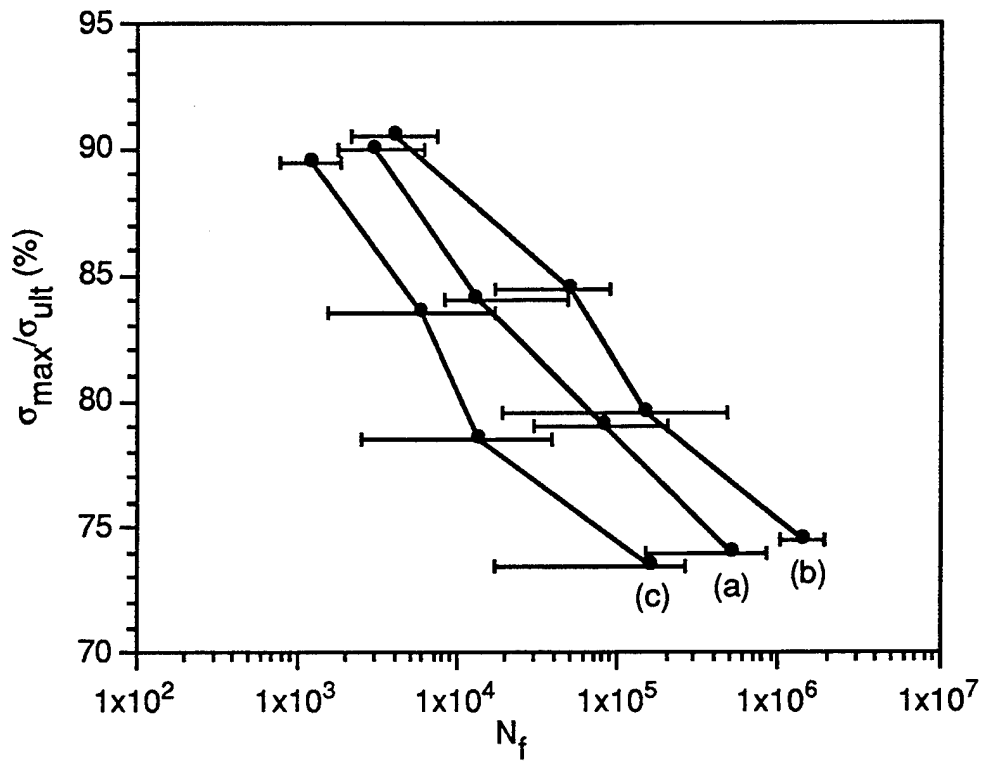Fig. 12   Mode I fracture energy as a function of applied stress for: (a) dry coupons fatigued in air, (b) saturated coupons fatigued in air, and (c) saturated coupons fatigued while immersed in sea water. (For a crack spacing of 10 mm and delamination of 0.125 mm.)

Fig. 13   Maximum total fracture energy as a function of delamination length for: (a) dry coupons fatigued in air, (b) saturated coupons fatigued in air, and (c) saturated coupons fatigued while immersed in sea water. (For fatigue in air this occurs at $\overline{\sigma}_x^{max}$, for immersed fatigue it occurs at $\overline{\sigma}_x^{min}$. Crack spacing is 10 mm.)

Fig. 14   Maximum mode I fracture energy as a function of delamination length for: (a) dry coupons fatigued in air, (b) saturated coupons fatigued in air, and (c) saturated coupons fatigued while immersed in sea water. (For fatigue in air this occurs at $\overline{\sigma}_x^{max}$, for immersed fatigue it occurs at $\overline{\sigma}_x^{min}$. Crack spacing is 10 mm.)

Fig. 1   A schematic diagram of an immersed fatigue test.
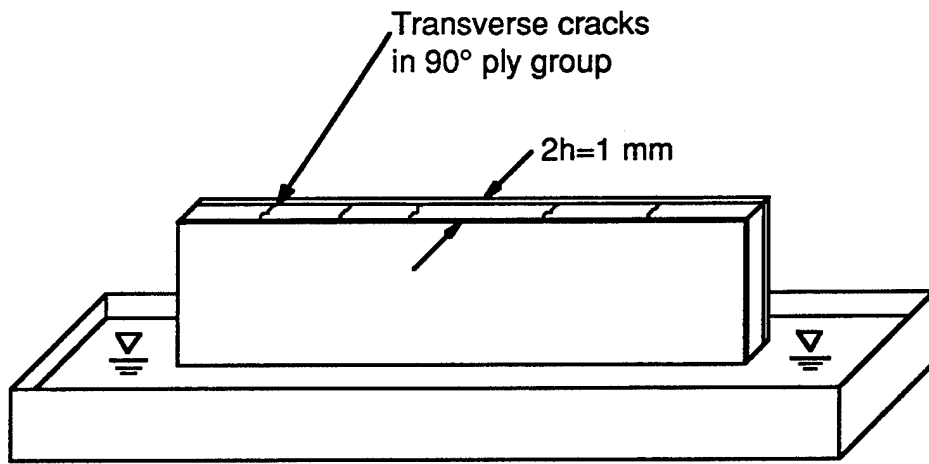
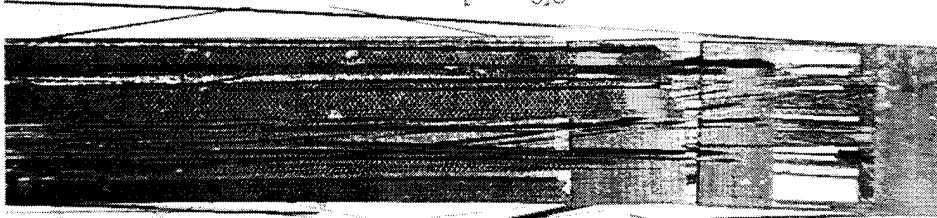Fig. 2   A schematic diagram of a capillary climb test.

Fig. 3   Fatigue life diagram for: (a) dry coupons fatigued in air, (b) saturated coupons fatigued in air, and (c) saturated coupons fatigued while immersed in sea water.

WET FATIGUE FAILURE SPECIMEN
MATERIAL : AS4/3501-6
LAY-UP : [0/90₃]s

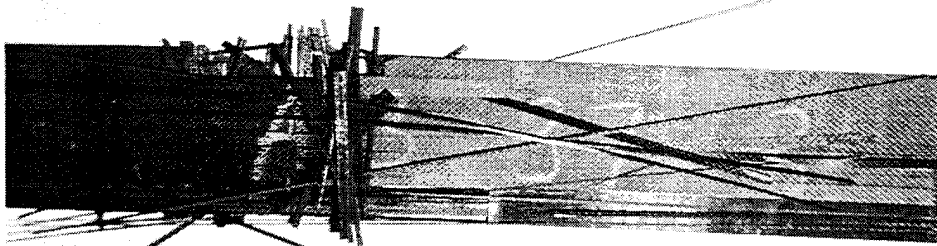DRY FATIGUE FAILURE SPECIMEN
MATERIAL : AS4/3501-6
LAY-UP : [0/90₃]s

Fig. 4   Top: photograph of saturated coupon fatigued while immersed in sea water. Bottom: photograph of dry coupon fatigued in air. Note the extensive delaminations in the immersed case and the higher density of transverse cracks in the dry case.
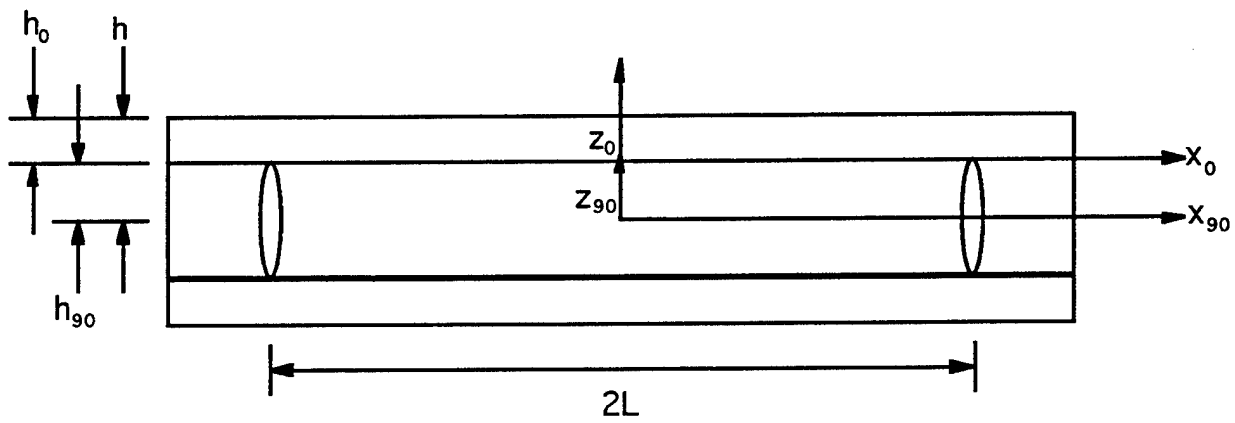
Fig. 5   Geometry and crack spacing assumed in the shear lag model.
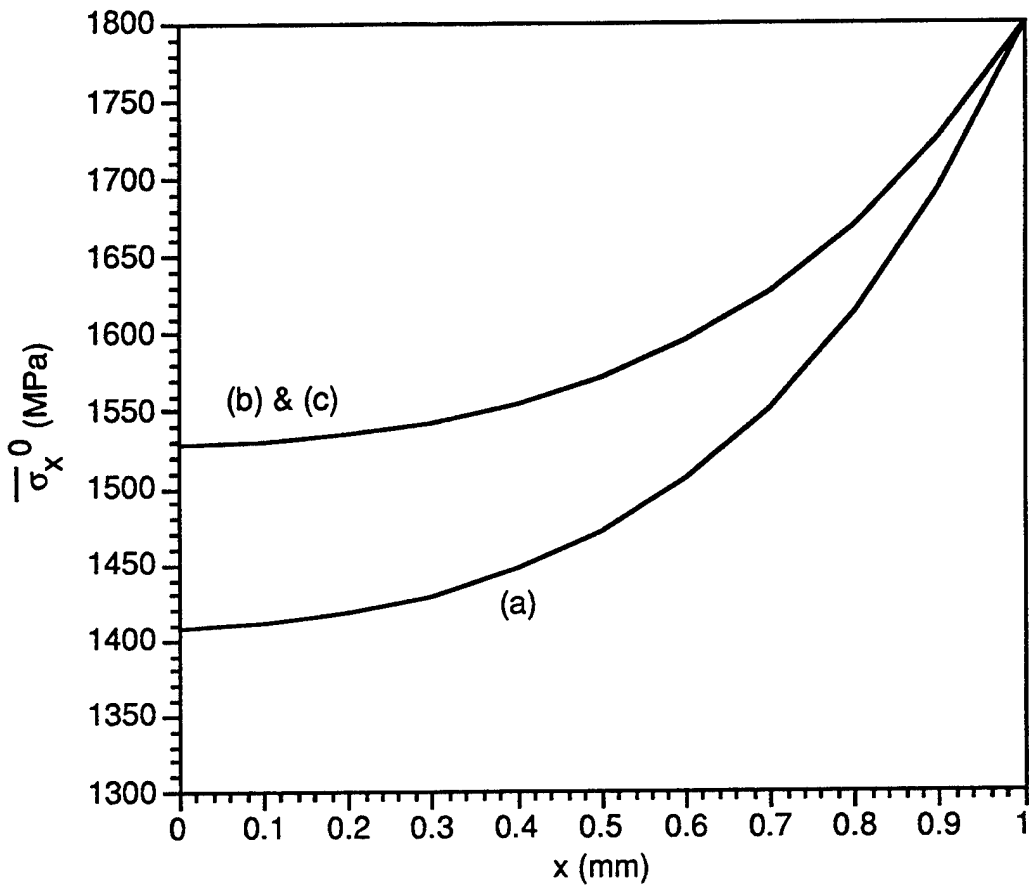
Fig. 6   Shear lag results of the average stress, $\overline{\sigma}_x^0$, in the outer 0° ply group vs. x at the maximum applied stress for: (a) dry coupons fatigued in air, (b) saturated coupons fatigued in air, and (c) saturated coupons fatigued while immersed in sea water. (For a crack spacing of 2 mm. Crack is located at x = 1 mm.)
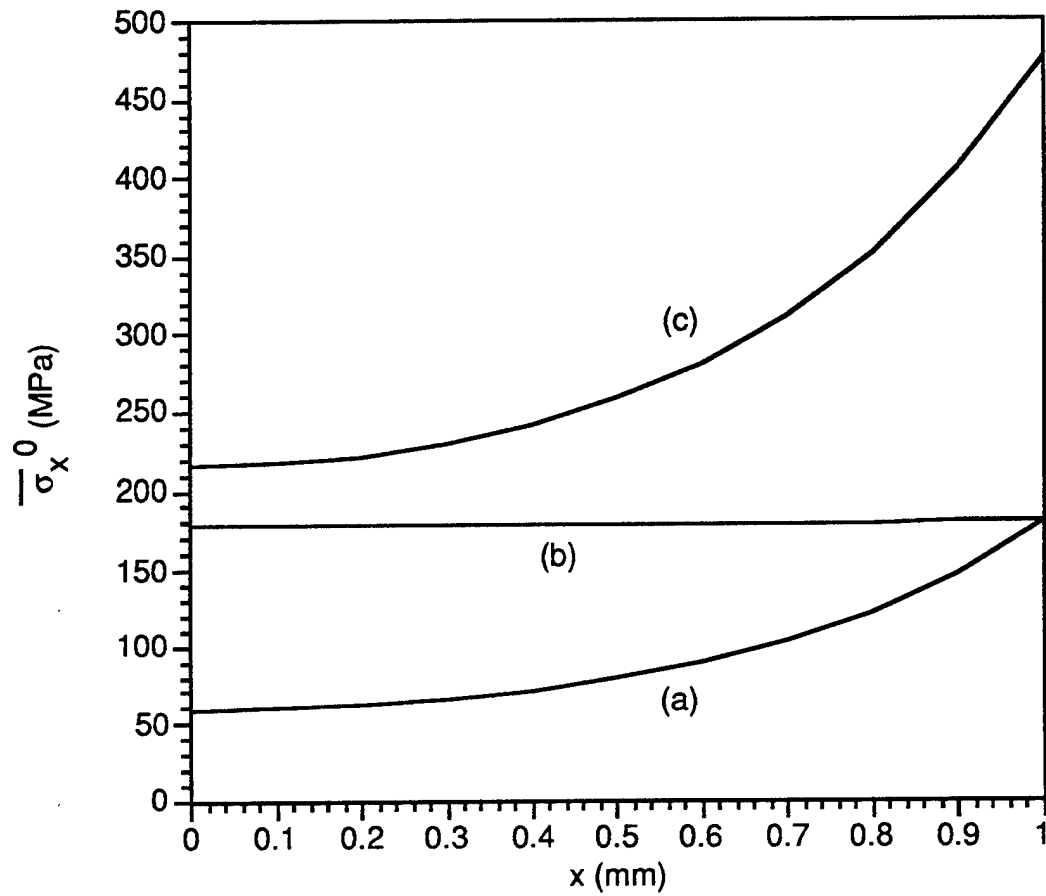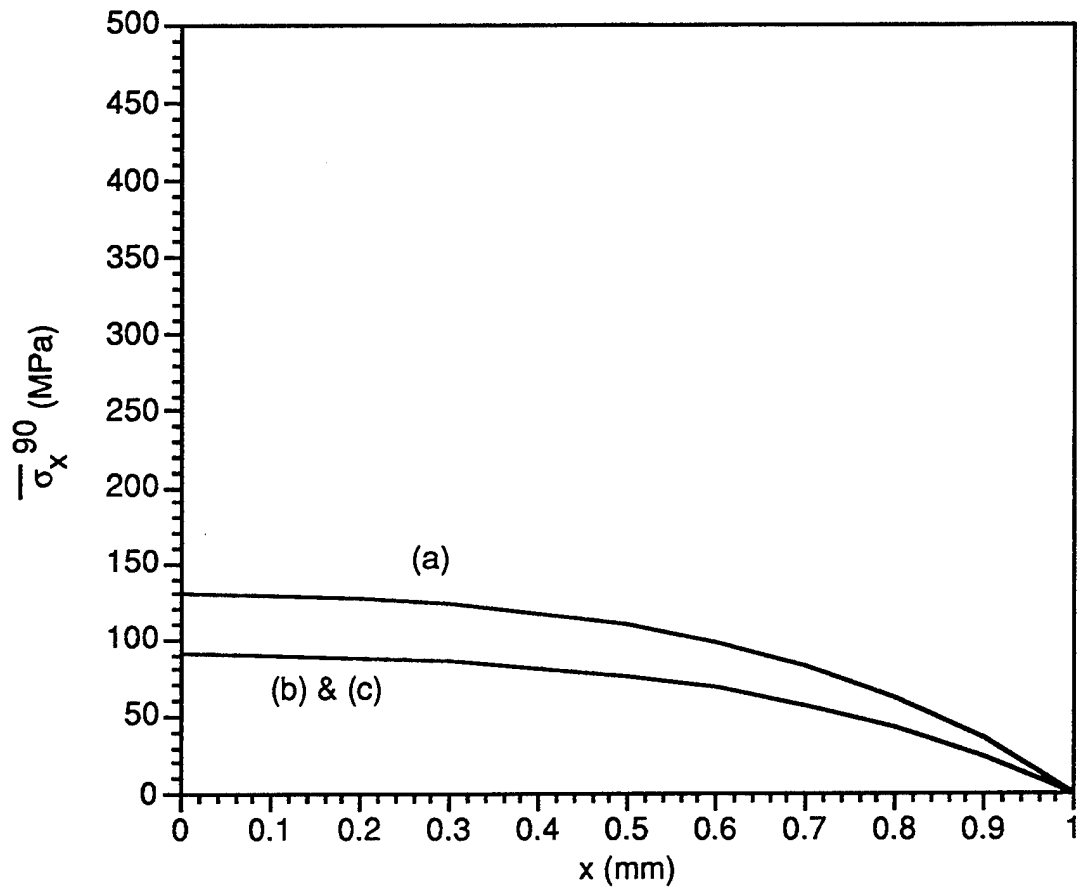
18

Fig. 7   Shear lag results of average stress, $\overline{\sigma}_x^0$, in the outer 0° ply group at the minimum applied stress for: (a) dry coupons fatigued in air, (b) saturated coupons fatigued in air, and (c) saturated coupons fatigued while immersed in sea water. (For a crack spacing of 2 mm. Crack is located at x = 1 mm.)
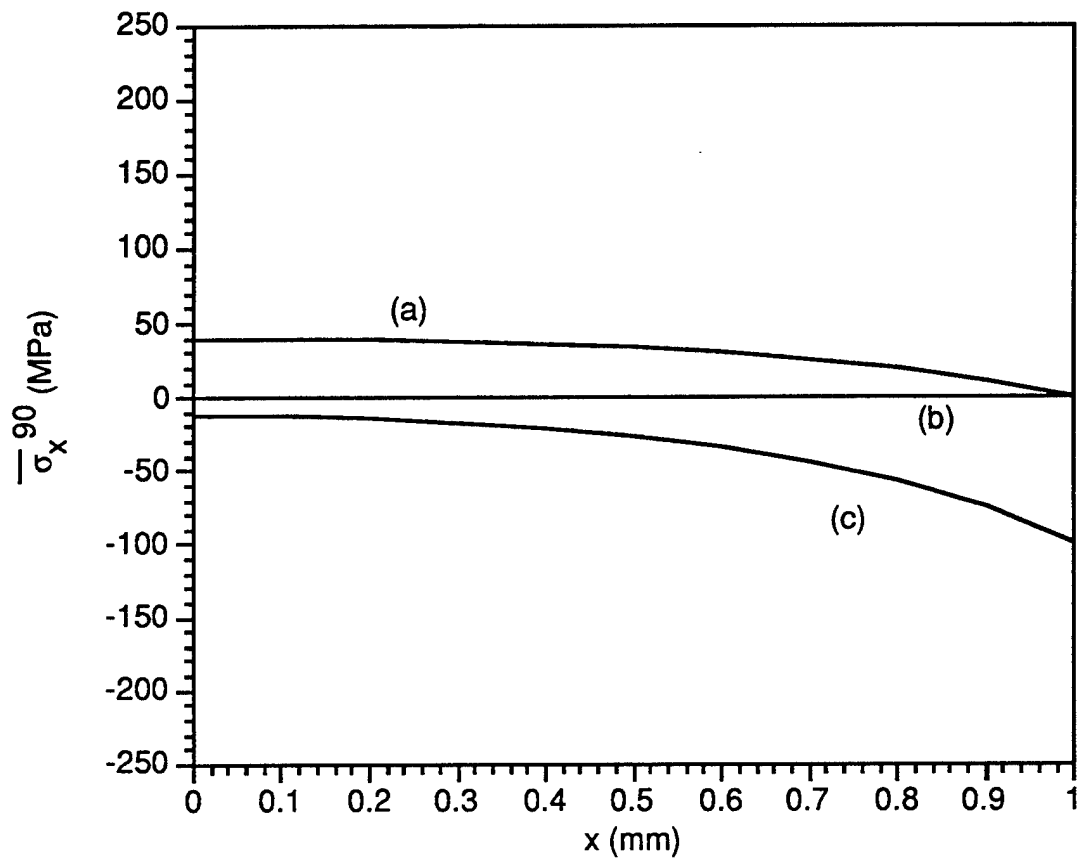
Fig. 8   Shear lag results of average stress, $\overline{\sigma}_x^{90}$, in the inner 90° ply group at the maximum applied stress for: (a) dry coupons fatigued in air, (b) saturated coupons fatigued in air, and (c) saturated coupons fatigued while immersed in sea water. (For a crack spacing of 2 mm. Crack is located at x = 1 mm.)

Fig. 9   Shear lag results of average stress, $\overline{\sigma}_x^{-90}$, in the inner 90° ply group at the minimum applied stress for: (a) dry coupons fatigued in air, (b) saturated coupons fatigued in air, and (c) saturated coupons fatigued while immersed in sea water. (For a crack spacing of 2 mm. Crack is located at x = 1 mm.) Note the compressive stresses within the 90° ply group in the saturated-immersed case in spite of the fact that $\overline{\sigma}_x^{-min}$ = +45 MPa.
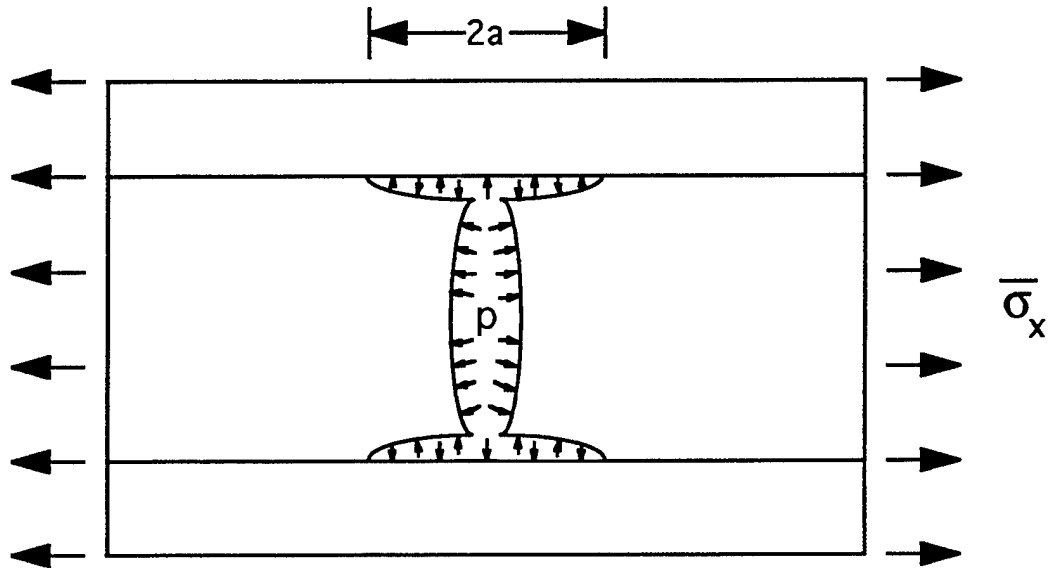
Fig. 10   Geometry of delaminated crack assumed in the finite element model.
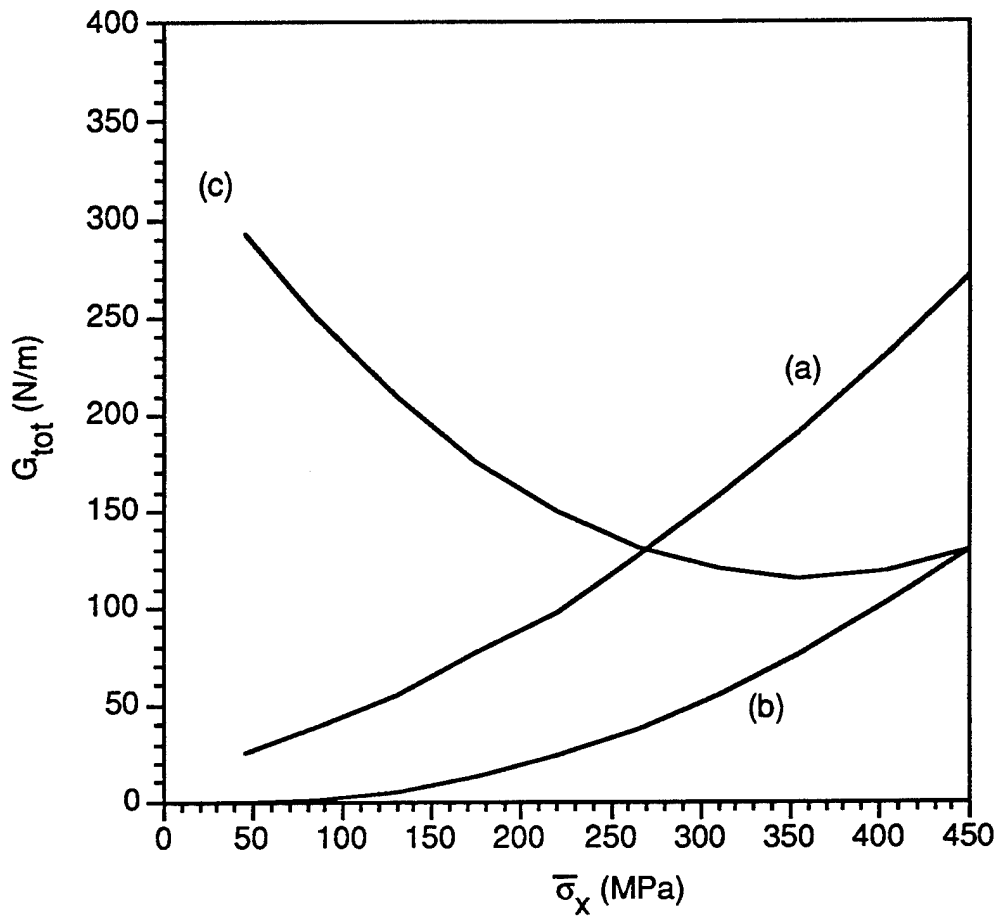
Fig. 11 Total fracture energy as a function of applied stress for: (a) dry coupons fatigued in air, (b) saturated coupons fatigued in air, and (c) saturated coupons fatigued while immersed in sea water. (For a crack spacing of 10 mm and delamination of 0.125 mm.)
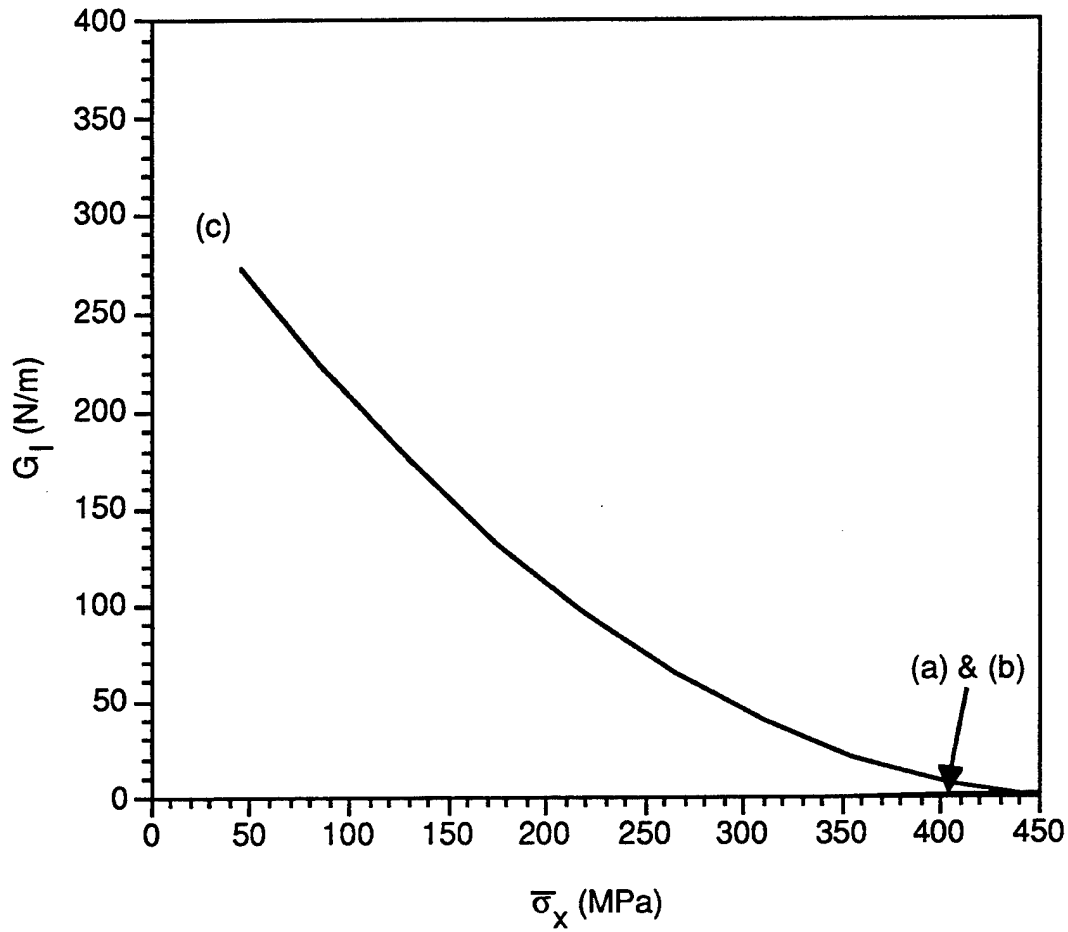
Fig. 12   Mode I fracture energy as a function of applied stress for: (a) dry coupons fatigued in air, (b) saturated coupons fatigued in air, and (c) saturated coupons fatigued while immersed in sea water. (For a crack spacing of 10 mm and delamination of 0.125 mm.)
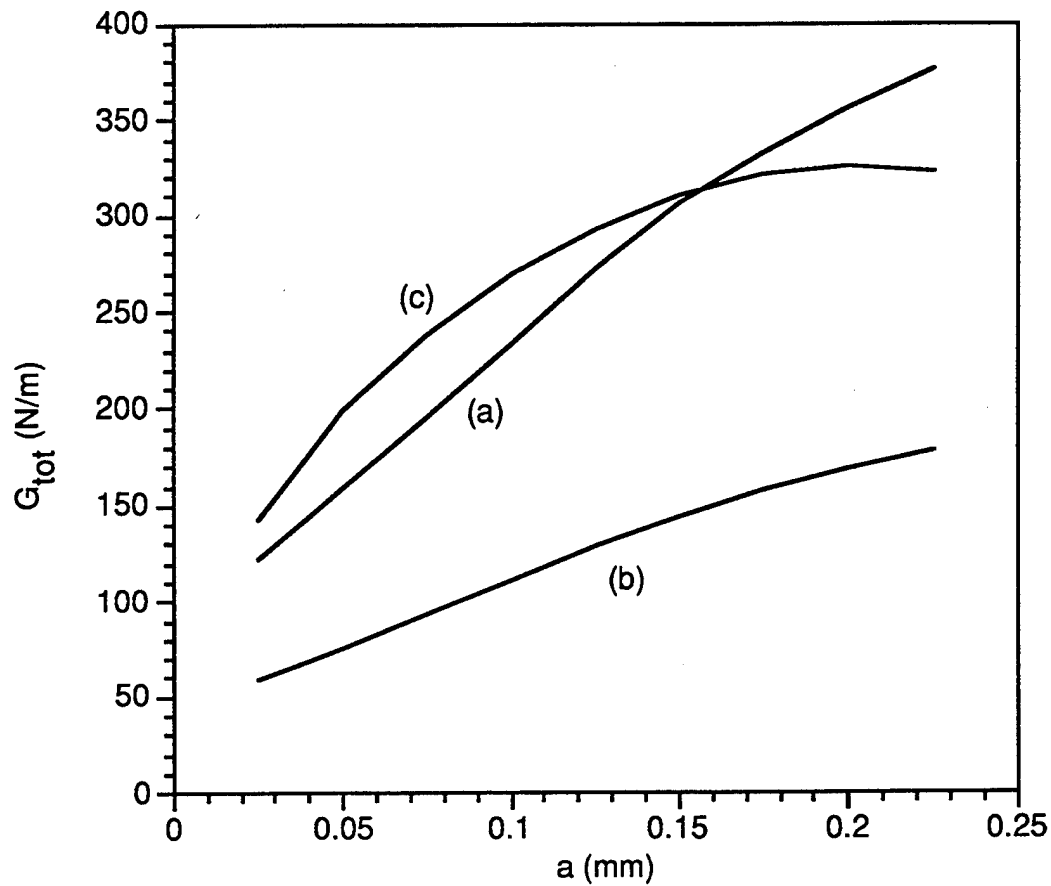
Fig. 13   Maximum total fracture energy as a function of delamination length for:
(a) dry coupons fatigued in air, (b) saturated coupons fatigued in air, and (c) saturated
coupons fatigued while immersed in sea water. (For fatigue in air this occurs at
$\overline{\sigma}_x^{max}$, for immersed fatigue it occurs at $\overline{\sigma}_x^{min}$. Crack spacing is 10 mm.)
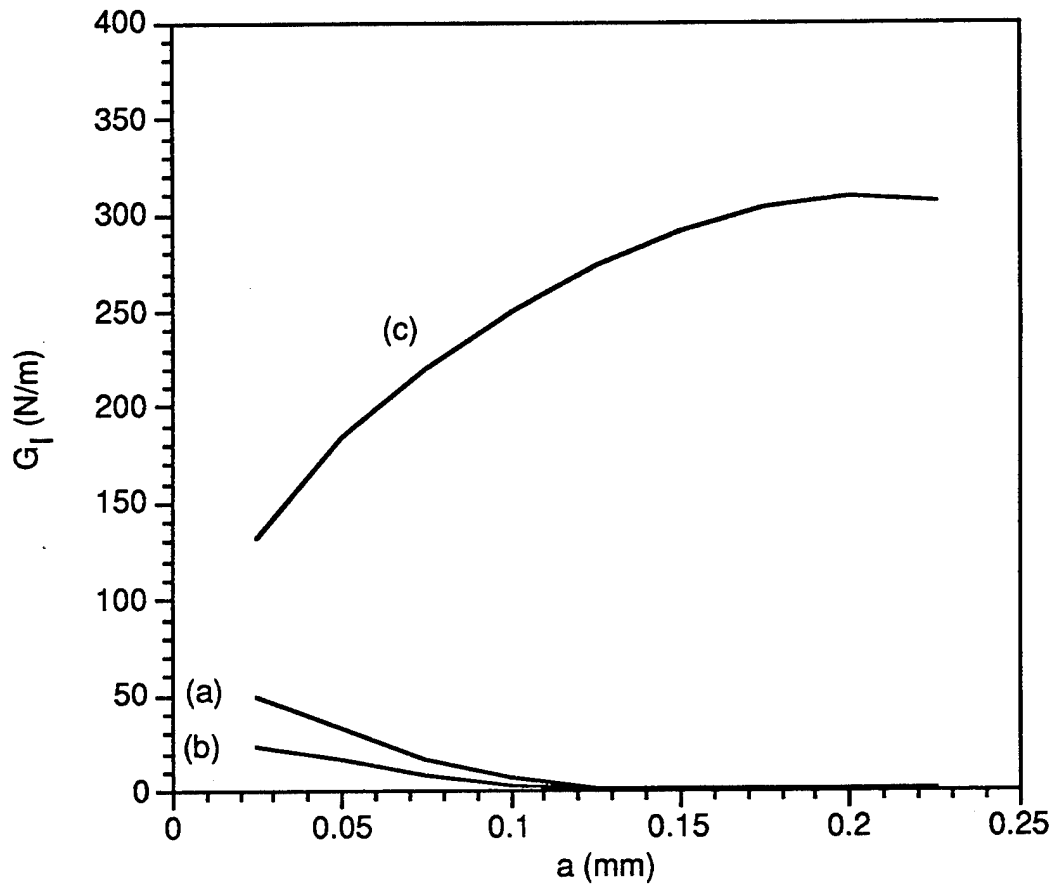
Fig. 14 Maximum mode I fracture energy as a function of delamination length for: (a) dry coupons fatigued in air, (b) saturated coupons fatigued in air, and (c) saturated coupons fatigued while immersed in sea water. (For fatigue in air this occurs at $\overline{\sigma}_x^{max}$, for immersed fatigue it occurs at $\overline{\sigma}_x^{min}$. Crack spacing is 10 mm.)